

*An alternative mechanism of pile failure in liquefiable deposits
during earthquakes*

CUED/D-SOILS/TR324 (Oct 2002)

By

**Subhamoy Bhattacharya
S.P.G.Madabhushi
Malcolm Bolton**

**This paper has been submitted to Geotechnique and is under
review.**

An alternative mechanism of pile failure in liquefiable deposits during earthquakes.

Subhamoy Bhattacharya, S.P.G.Madabhushi and Malcolm Bolton

University of Cambridge, UK

ABSTRACT

This paper proposes an alternative pile failure mechanism in liquefiable deposits during earthquakes. This failure mechanism, based on pile buckling, is formulated by back analysing 15 case histories of pile foundation performance during earthquakes and verified using dynamic centrifuge tests. A new parameter, the slenderness ratio of a pile is introduced to classify pile performance in liquefiable soils. This parameter fits very well the reported case histories and the centrifuge test results.

INTRODUCTION

There has been confusion among engineers about the mechanism of pile failure following the collapse of some piled foundations during the 1995 Kobe earthquake. The failure modes of piles observed were quite similar to the observations after earlier earthquakes e.g. the 1964 Niigata earthquake. The current understanding of pile failure is as follows. Soil liquefies, losing its shear strength, causing it to flow taking with it any overlying non-liquefied crust. These soil layers drag the pile with them, causing a bending failure. This is often referred to as failure due to lateral spreading. In terms of soil pile interaction, the current mechanism of failure assumes that the soil pushes the pile. The Japanese Highway code of practice (JRA 1996) has codified this concept.

While this mechanism appears plausible, this paper proposes a different pile failure mechanism, which focuses on the slenderness of piles. The loss of support from the surrounding liquefied soil can cause a pile to become unstable under axial load, provided the slenderness ratio of the pile in the unsupported zone exceeds a critical value. This instability can cause the pile to buckle sideways, eventually causing a plastic hinge in the pile. In terms of soil-pile interaction, the proposed mechanism assumes that, during instability, the pile pushes the soil. In this paper, this hypothesis of pile failure has been investigated by back analysing 15 case histories of pile

foundation performance during past earthquakes and carrying out four dynamic centrifuge tests.

STUDY OF CASE HISTORIES

Structurally, axially loaded piles are long slender columns with lateral support from the surrounding soil. If unsupported, these columns will fail in buckling instability and not due to crushing of the material. Fig 1 shows the length and diameter of tubular piles used in different projects around the world after Bond (1989). The figure shows that piles normally have ratios of length to diameter of 25 to 100. In this paper we will introduce the parameter r_{\min} (minimum radius of gyration) to analyse the piles in the reported case histories and centrifuge tests. This parameter can represent piles of any shape (square, tubular or circular) and is used by structural engineers for studying buckling instability.

$$I = A.r_{\min}^2 \quad \text{or,} \quad r_{\min} = \sqrt{\frac{I}{A}} \quad (1)$$

where:

I = second moment area of the pile section about the weakest axis (m^4).

A = area of the pile section (m^2).

r_{\min} = minimum radius of gyration of the pile section about any axis of bending (m).

The formula for calculating r_{\min} for various pile sections is shown in Appendix 1. For a tubular pile r_{\min} is 0.35 times of the outside diameter and hence from figure 1, the length (L) to r_{\min} ratio of normal piles ranges from 71 to 284.

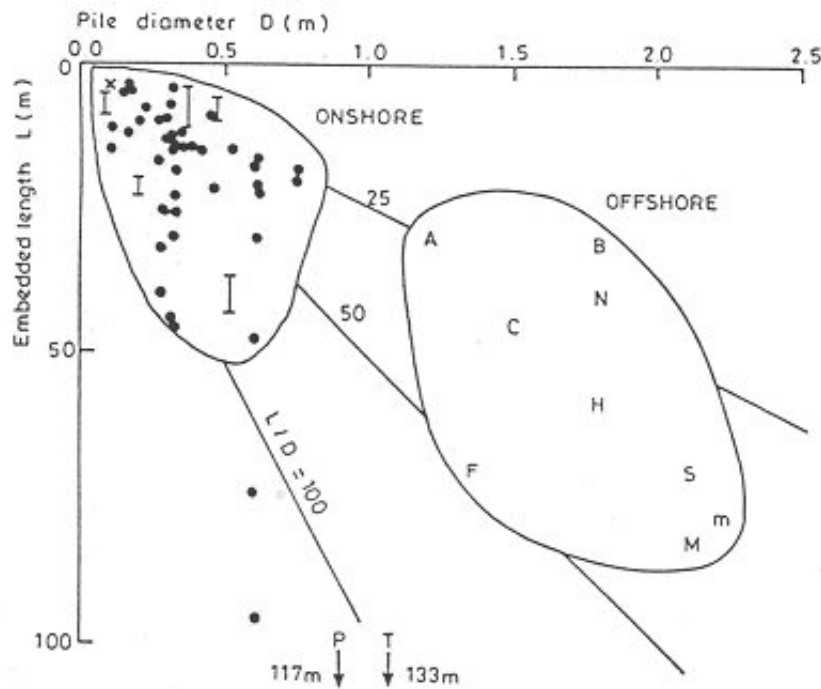


Figure 1: Length and diameter of tubular piles, Bond (1989).

A significant number of cases of pile performance during earthquake liquefaction have been reported in the literature. Some pile foundations were found to survive the earthquake while others suffered severe damage. Fifteen cases of pile foundation performance are analysed and presented in table 1, giving emphasis to buckling characteristics. The parameters in the analysis are

1. L_{eff} = Effective length of the pile in the liquefiable region. The definition of effective length shown in figure 2 has been adopted from column stability theory and is chosen to normalise the different boundary conditions of pile tip and pile head. L_{eff} is also familiar as the “Euler’s buckling length” of a strut pinned at both ends. In practice, designers may prefer to adjust effective length slightly to account for imperfect fixity, especially in reinforced concrete; e.g Tomlinson (1977).
2. r_{min} = minimum radius of gyration of the pile.
3. Slenderness ratio of the pile in liquefiable region, L_{eff}/r_{min} .
4. Allowable load on the pile, P , based on conventional design procedures, with no allowance for liquefaction.
5. Euler’s elastic critical load of the pile (P_{cr}) calculated from the well-known buckling formula as shown by equation 2.

$$P_{cr} = \frac{\pi^2}{L_{eff}^2} EI \quad (2)$$

6. Axial stress σ in the pile, calculated by dividing P by the cross-sectional area of the pile, A . The value at failure is written as σ_f .

A sample calculation of a particular case history is given in Appendix 2. Figure 3 shows the effective length of the piles in a liquefiable zone plotted against the r_{min} of the pile section. A line representing a slenderness ratio (L_{eff}/r_{min}) of 50 is drawn and it distinguishes poor performance piles from the good ones. This line is of some significance in structural engineering, as it is often used to distinguish between “long” and “short” columns. Columns having slenderness ratios below 50 are expected to fail in crushing whereas those above 50 are expected to fail in buckling instability.

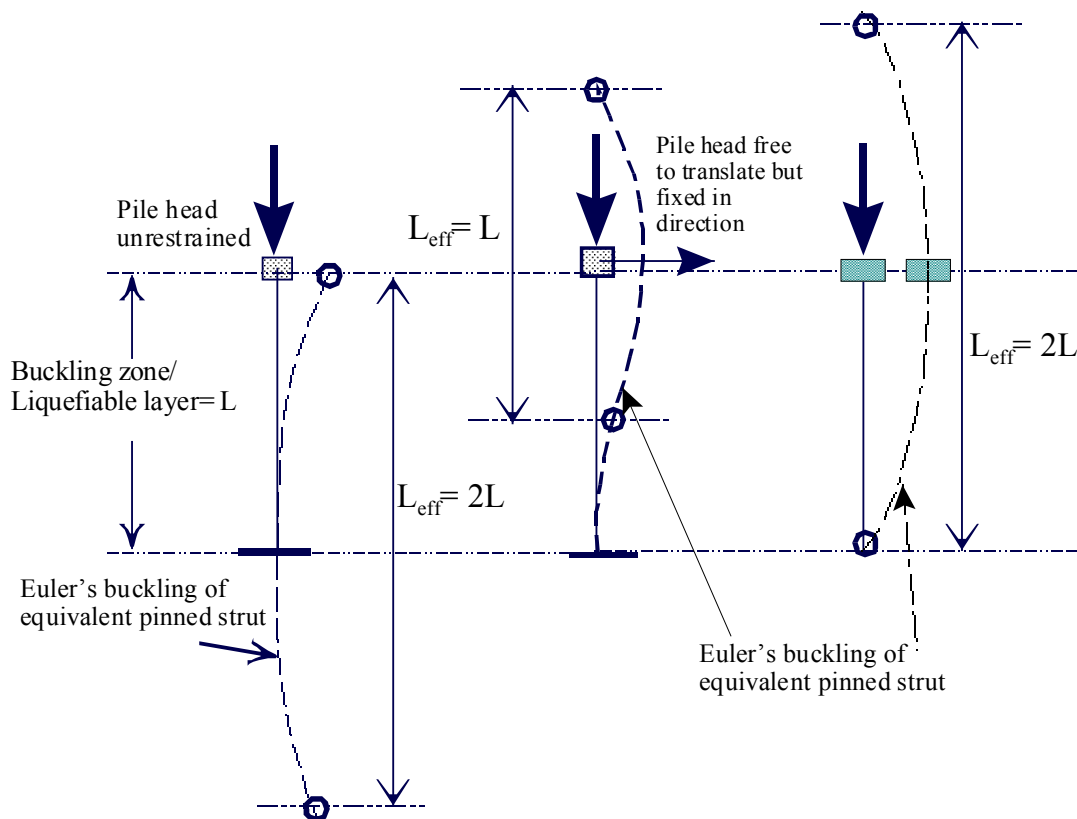


Figure 2: Concept of effective length of pile.

Table 1: Summary of pile performances

Sl no.	Case History and Reference.	L^* (m)	L_0^{**} (m)	Pile section /type	Framing action/ β^{***} value	L_{eff} (m)	r_{min} (m)	L_{eff}/r_{min}	P MN	P_{cr} MN	σ MPa	Lateral spreading observed?	Performance
1	10 storey-Hokuriku building, 1964 Niigata earthquake, Hamada (1992)	12	5	0.4m dia RCC	Large piled raft with basement. 1	5.0	0.1	50	0.77	12.4	6.2	Yes, nearby ground moved by 2m.	Good
2	Landing bridge, 1987 Edgecumbe earthquake, Berrill et al (2001)	9	4	0.4m square PSC	Raked piles, no sway frame 0.5	2.0	0.12	17	0.62	139	3.8	Yes, ground cracked and sand ejected.	Good
3	14 storey building in American park, 1995 Kobe earthquake, Tokimatsu et al (1996)	33	12.2	2.5m dia RCC	Large pile group and large pile dia. 1.0	12.2	0.63	19	19	3183	3.8	Yes, quay walls on the west, south and east moved.	Good
4	Kobe Shimim hospital, 1995 Kobe earthquake, Soga (1997)	30	6.2	0.66m dia Steel tube	Large piled raft with basement. 1.0	6.2	0.23	27	3.0	91	92.6	No, Ground subsided.	Good
5	Hanshin expressway pier, 1995 Kobe earthquake, Ishihara (1997)	41	15	1.5m dia RCC	Small group (22 piles) 1.0	15	0.38	40	14	272	7.9	Yes, ground moved by 0.62m.	Good
6	LPG tank 101, Kobe earthquake, Ishihara (1997)	27	15	1.1m dia RCC	Large piled raft 1.0	15	0.28	53	4.1	79	4.3	Yes, ground moved by 0.7m.	Good
7	N.H.K building, 1964 Niigata earthquake, Hamada (1992)	12	10	0.35m dia RCC	Groups tied by flexible beam, Less embedment at pile tip. 2.0	20	0.09	222	0.43	0.45	4.4	Yes, nearby ground moved by 2m.	Poor
8	NFCH building, 1964 Niigata earthquake, Hamada (1992)	9	8	0.35m dia RCC hollow	Groups tied by flexible beam, Less embedment at pile tip 2.0	16	0.10	160	0.29	0.63	4.5	Yes, nearby ground moved by 1 to 2m.	Poor

Sl no.	Case History and Reference.	L* (m)	L ₀ ** (m)	Pile section /type	Framing action/ β *** value	L _{eff} (m)	r _{min} (m)	L _{eff} /r _{min}	P MN	P _{cr} MN	σ MPa	Lateral spreading observed?	Performance
9	Showa bridge, 1964 Niigata earthquake, Hamada (1992)	25	19	0.6m dia Steel tube	A single row of piles 2.0	38	0.21	181	0.96	1.10	56.3	Yes, width of river decreased.	Poor
10	Yachiyo Bridge, 1964 Niigata earthquake, Hamada (1992)	11	8	0.3m dia RCC	Isolated footing 2.0	16	0.08	200	0.34	0.39	4.8	Yes, width of river decreased.	Poor
11	Gaiko Ware House, 1983 Chubu earthquake, Hamada (1992)	18	14	0.6m dia PSC hollow	Isolated footing 2.0	28	0.16	175	1.47	1.61	9.3	Yes, nearby ground moved by 1.5m.	Poor
12	4 storey fire house, 1995 Kobe earthquake, Tokimatsu et al (1996)	30	18	0.4m dia PSC	Groups tied by beam. 1.0	18	0.10	180	0.89	0.96	7.0	Yes, building moved and tilted towards the sea.	Poor
13	3 storied building at Fukae, 1995 Kobe earthquake, Tokimatsu et al (1998)	20	16	0.4m dia PSC hollow	Groups tied by beam. 1.0	16	0.12	133	0.72	1.02	9.4	Yes, building moved and tilted towards the sea.	Poor
14	Elevated port liner railway, 1995 Kobe earthquake, Soga (1997)	30	12	0.6m dia RCC	Isolated footing, large embedment at pile tip. 1.0	12	0.15	80	1.38	10.92	4.9	Yes,	Poor, cracks were seen in the piles.
15	LPG tank 106,107 –1995 Kobe earthquake, Ishihara (1997)	20	15	0.3m dia RCC hollow	Groups tied by beams. 1.0	15	0.08	187	0.46	0.38	6.6	No, ground subsided.	Poor

* L = Length of the pile;

** L₀ = Length of pile in liquefiable region/ buckling zone.

*** β = Factor for estimating effective length. L_{eff} = β L₀.

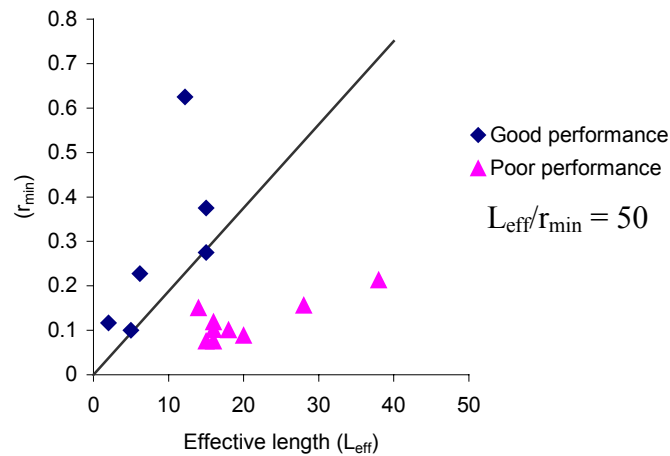


Figure 3: L_{eff} versus r_{min} for piles studied

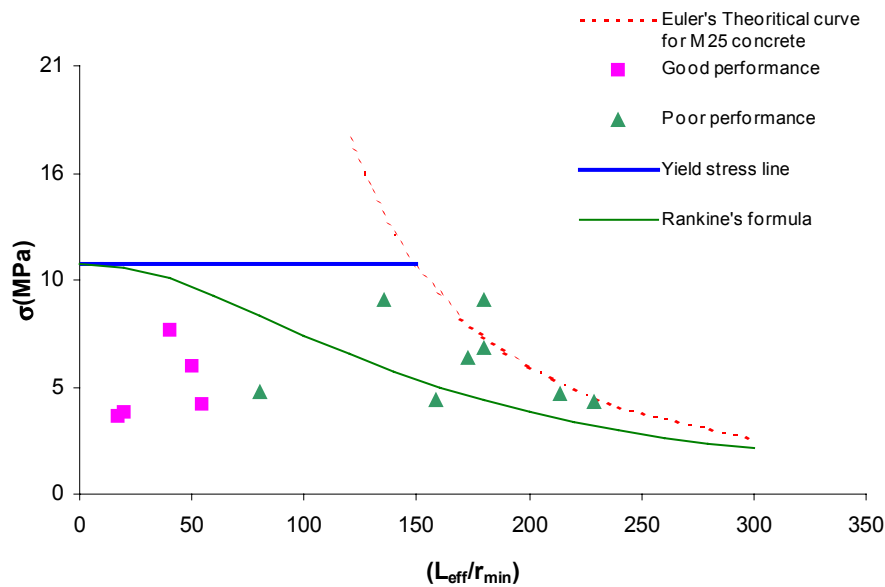


Figure 4: Plot of concrete pile performance mentioned in table 1.

Figure 4 shows the plot of 13 concrete piles mentioned in table 1. The piles are assumed to be of M25 grade concrete (BS 8110), with a characteristic strength of 25 MPa. In the plot, three well-defined lines are drawn viz.

- Yield stress line ($\sigma_y = 11.2$ MPa) taken as the design crushing value,
- Euler's curve for σ_{cr} , which is the elastic stability limit from equation 3.
- A curve for σ_f drawn using Rankine's formula (1866) shown by equation 4.

This design curve mediates the transition between strength and stability. Many

other similar curves, such as Perry-Robertson (1886&1925), can equally be used.

Substituting the value of I from equation 1 into equation 2 and noting that σ_{cr} is the critical stress given by (P_{cr}/A), the following equation is obtained.

$$\sigma_{cr} = \frac{P_{cr}}{A} = \frac{\pi^2}{\left(\frac{L_{eff}}{r_{min}}\right)^2} E \quad (3)$$

which leads to

$$\frac{1}{\sigma_f} = \frac{1}{\sigma_{cr}} + \frac{1}{\sigma_y} \quad (4)$$

where σ_y is yield stress of the material and σ_{cr} is the elastic critical stress as calculated by equation 3, leading to an estimate of the combined failure stress σ_f .

HYPOTHESIS ARISING FROM THE STUDY OF CASE HISTORIES

The study of the case histories seems to show a dependence of pile performance on buckling parameters. As short columns fail in crushing and long columns in buckling, the analysis suggests that pile failure in liquefied soils is similar in some ways to the failure of long columns in air. The lateral support offered to the pile by the soil prior to the earthquake is removed during liquefaction. This hypothesis is shown in figure 5 and explained below.

During earthquakes, soil layers overlying the bedrock are subjected to seismic excitation consisting of numerous incident waves, namely shear (S) waves, dilatational or pressure (P) waves, and surface (Rayleigh and Love) waves which result in ground motion. The ground motion at a site will depend on the stiffness characteristics of the layers of soil overlying the bedrock. This motion will also affect a piled structure. As the seismic waves arrive in the soil surrounding the pile, the soil layers will tend to deform. This seismically deforming soil will try to move the piles and the embedded pile-cap with it. Subsequently, depending upon the rigidity of the

superstructure and the pile-cap, the superstructure may also move with the foundation. The pile may thus experience two distinct phases of initial soil-structure interaction.

1. Before the superstructure starts oscillating, the piles may be forced to follow the soil motion, depending on the flexural rigidity (EI) of the pile. Here the soil and pile may take part in kinematic interplay and the motion of the pile may differ substantially from the free field motion. This may induce bending moments in the pile.
2. As the superstructure starts to oscillate, inertial forces are generated. These inertia forces are transferred as lateral forces and overturning moments to the pile via the pile-cap. The pile-cap transfers the moments as varying axial loads and bending moments in the piles. Thus the piles may experience additional axial and lateral loads, which cause additional bending moments in the pile.

These two effects occur with only a small time lag. If the section of the pile is inadequate, bending failure may occur in the pile. The behaviour of the pile at this stage may be approximately described as a beam in an elastic foundation, where the soil provides sufficient lateral restraint. The available confining pressure around the pile is not expected to decrease substantially in these initial phases. The response to changes in axial load in the pile would not be severe either, as shaft resistance continues to act. This is shown in figure 5 (b).

In loose saturated sandy soil, as the shaking continues, pore pressure will build up and the soil will start to liquefy. With the onset of liquefaction, an end-bearing pile passing through liquefiable soil will experience distinct changes in its stress state.

- The pile will start to lose its shaft resistance in the liquefied layer and shed axial loads downwards to mobilise additional base resistance. If the base capacity is exceeded, settlement failure will occur.
- The liquefied soil will begin to lose its stiffness so that the pile acts as an unsupported column as shown in figure 5(c). Piles that have a high slenderness ratio will then be prone to axial instability, and buckling failure may occur in the pile, enhanced by the actions of lateral disturbing forces and also by the deterioration of bending stiffness due to the onset of plastic yielding.

In sloping ground, even if the pile survives the above load conditions, it may experience additional drag load due to the lateral spreading of soil. Under these conditions, the pile may behave as a beam-column (column with lateral loads); see Figure 5d.

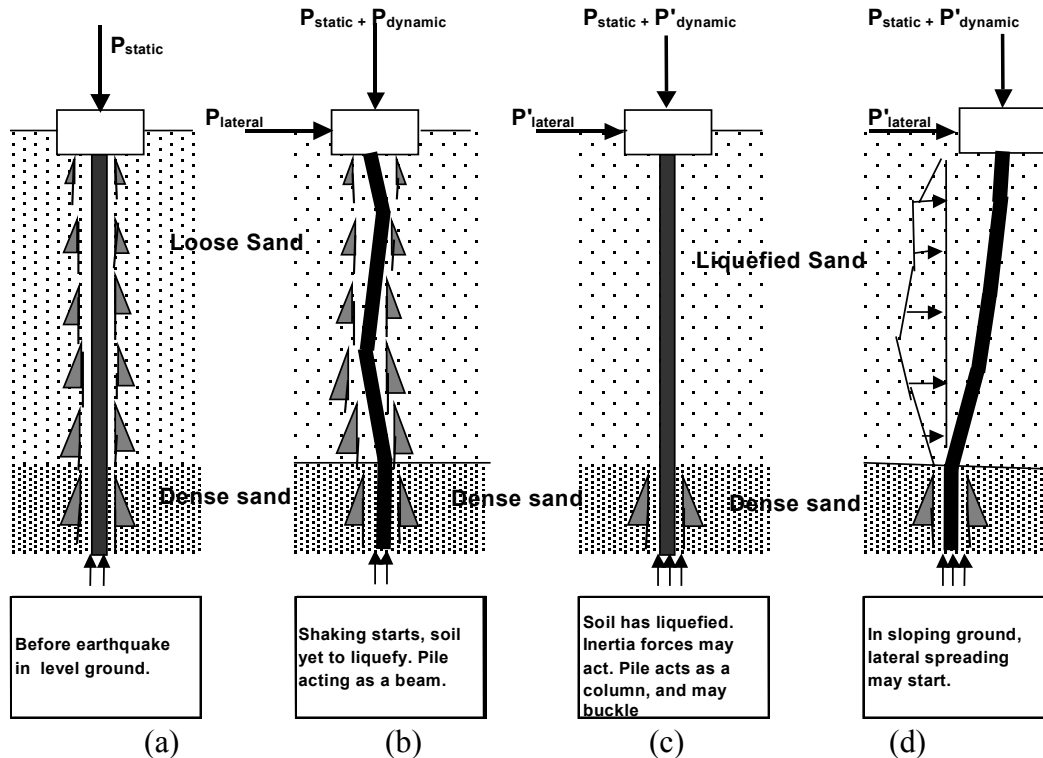


Figure 5: The time history of loading in the proposed failure mechanism.

DYNAMIC CENTRIFUGE MODELLING AND MODEL LAYOUT

Dynamic centrifuge modelling is regarded as an appropriate tool to test the new hypothesis of pile failure irrespective of lateral drag. The 10m-beam centrifuge at the Schofield Centre of Cambridge University Engineering Department (CUED) was used to perform the centrifuge tests. Details of the centrifuge and the applicable scaling laws can be found in Schofield (1980) and Schofield (1981). A mechanical shaking table known as the Stored Angular Momentum (SAM) earthquake actuator developed at Cambridge University (Madabhushi et al., 1998), was used to impart in-flight earthquake loading to the physical models.

In a full-scale structure, piled foundations rest within a soil that is unbounded laterally. In order to simulate an analogous situation in the centrifuge model, a specially designed model container known as the ESB (Equivalent Shear Beam) box has been used. The container has inside dimensions of 560mm × 235mm × 220mm

(deep) and its boundary wall is designed to have the same dynamic stiffness as that of unliquefied soil in the free field. Details of the design of the box can be seen in Schofield and Zeng (1992).

Four model tests (SB-02, SB-03, SB-04 and SB-05) were carried out at 1: 50 scale and at 50-g (i.e. at fifty times the earth gravities) to study the problem of pile failure. Experiments were designed in level ground to avoid the effects of drag due to lateral spreading. The main aim was to study the effect of axial load on a pile as the soil liquefies. Eleven piles were tested in the four tests performed. The model pile is made of dural alloy tubes, the properties of which are given in table 2. A schematic diagram showing the basic principle of the experiments is shown in figure 6. A block of brass fixed at the pile head as shown in figure 7 is used to simulate the axial load in the pile in all the tests. With the increase in centrifugal acceleration to N -g, the brass weight imposes increasing axial force in the pile as shown in figure 6. One problem of using a brass weight is the action of Earth's gravity by which the resultant load acting on a radial pile is not purely axial. At lower g -levels especially, the soil may not gain enough confining pressure to prevent the pile deflecting under disproportionately large lateral forces, and the experiment may therefore begin by inducing an initial imperfection.

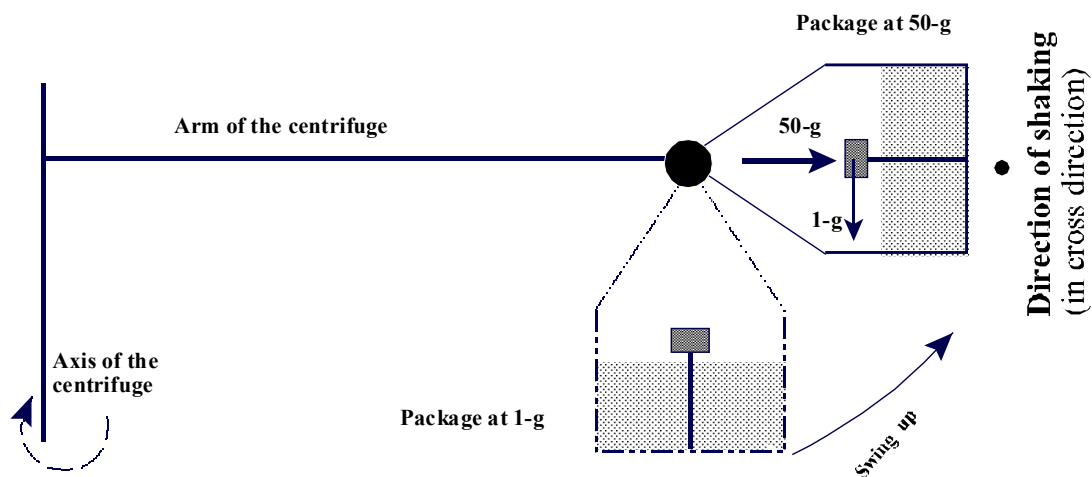


Figure 6: The forces that act on the model pile.

Following figure 6, there are three load effects, which control the failure mechanism in the centrifuge:

1. 1-g effect of Earth's gravity on the pile head mass,
2. N -g effect of centrifuging the pile head mass,
3. Inertia force induced during earthquake shaking.

A typical layout of a model is shown in figure 8. Table 3 summarises the four tests stating the parameters involved. It may be noted that through the sequence of tests the above-mentioned loading effects were successfully decoupled. In test SB-02, all three effects were present while in test SB-04 only the effect of axial load was studied. The effect of 1-g was countered in tests SB-03, SB-04 and SB-05 by fixing the bottom of the pile in a wedge at a slope 1 in 50 as shown in figure 7. This corrects the imperfection in simulated gravity and imposes a purely axial load in the pile at 50-g. In test SB-04, a specially designed frame was used to restrain the head mass against inertial action as shown in figure 9. Thus the pile is only allowed to move in a transverse direction orthogonal to the direction of shaking. Also, while the wedge corrects the 1-g effect at 50-g, at lower g levels the load acting is still not purely axial. So as to avoid premature failure while the g-level is being increased, a retractable pneumatic piston was used to hold the head mass temporarily. The pressure in the piston was released when the package reached 50-g and the pile remained stable. Lateral shaking was then imparted to the model. Test SB-04 was repeated as SB-05, but without soil. Therefore, the various influences on pile behaviour could be distinguished.

Fraction E silica sand prepared to a relative density of 45% was used for each model. Table 4 shows the properties of the sand. To have a consistent scaling law for time in inertial problems featuring pore pressure generation and dissipation, the viscosity of the pore fluid must be scaled up. Silicone oil was used, having a viscosity 50 times that of water.

Miniature instruments such as pore pressure transducers (PPT) and accelerometers (ACC) were buried in the model to obtain the soil response. An earthquake of 0.5 to 0.9 sec duration, 50 Hz frequency, and of lateral intensity 5g, was fired in the tests, which would correspond to 25 sec to 45 sec duration of a 1 Hz frequency earthquake of peak bedrock acceleration 0.1g at prototype scale.

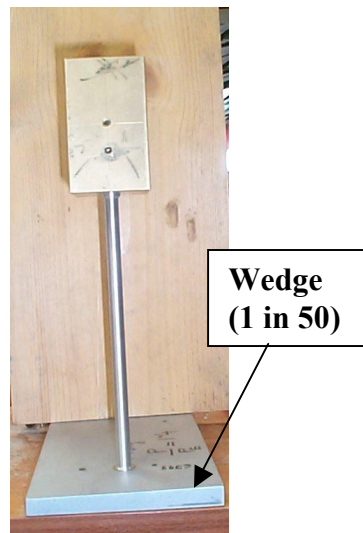


Figure 7: Method adopted to simulate axial load in pile and to minimise the 1-g effect.

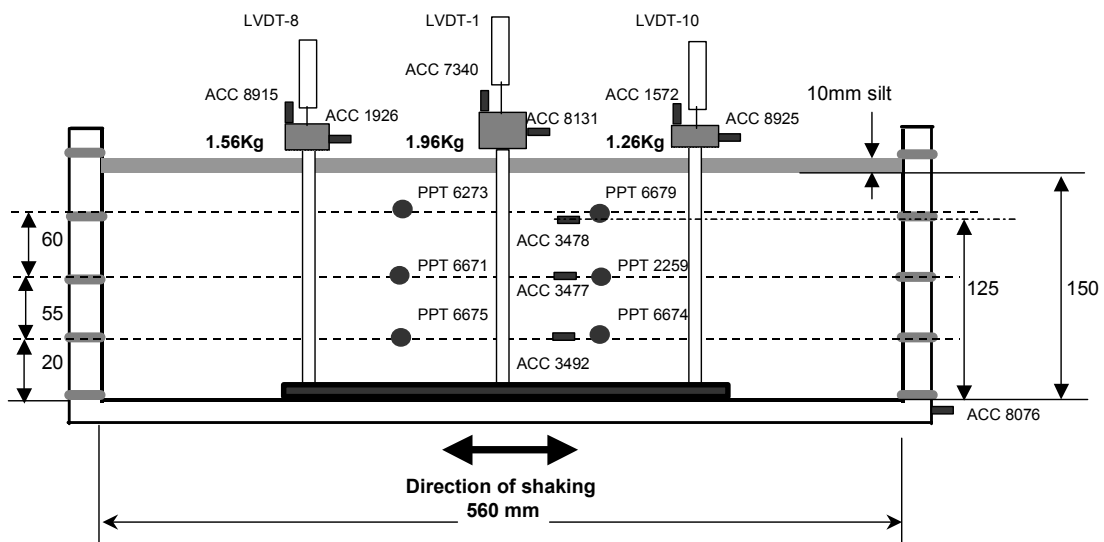


Figure 8: Model layout and instrumentation in test SB-02

Table-2: Properties of model pile

Material	Aluminum Alloy (Dural)
E (Young's Modulus)	70 GPa
Outside diameter	9.3 mm (9.2 mm in test SB-02)
Inside diameter	8.5 mm
r_{\min} of the section	3.1 mm
Yield Stress (measured)	250 MPa
Plastic moment capacity (M_p)	8175 Nmm
EI of the section	7.77×10^6 Nmm ²

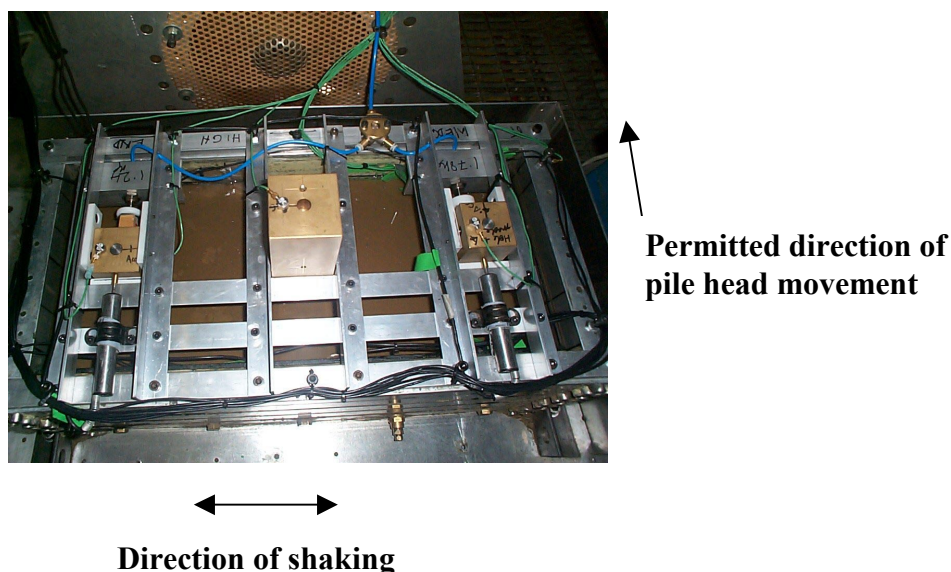


Figure 9: Test SB-04 with guides to hold the masses against inertia force.

Table 3: Summary of the tests

Test ID	Parameters involved in the test	Remarks
SB-02 (with soil)	1-g effect, axial load and inertial effects	Two piles failed during swing up due to 1-g effect.
SB-03 (with soil)	The effect of axial load and inertia load	1-g effect removed by wedge
SB-04 (with soil)	Only the effect of axial load	1-g and inertial effects removed
SB-05 (no soil)	Only the effect of axial load	1-g and inertial effects removed

Table 4: Properties of Fraction E sand (after Tan 1990)

D ₁₀ grain size	0.095 mm
D ₅₀ grain size	0.14 mm
D ₆₀ grain size	0.15 mm
Specific Gravity G _s	2.65
Minimum Void ratio e _{min}	0.613
Maximum Void ratio e _{max}	1.014
Permeability to water (e = 0.72)	0.98 E -04 m/s
Angle of shearing resistance at critical state φ _{crit}	32 ⁰ (estimated value)

In all the tests the models were fully prepared at 1-g, thus pile installation effects were not considered. The piles were fixed in place in the ESB box and sand was poured uniformly in layers by air-pluviation from an overhead hopper. After the completion of sand pouring, the model was fully saturated by silicone oil. The pile head masses were so designed that the axial loads applied to the piles at 50-g were arranged around

Euler's elastic critical load (P_{cr}) assuming the pile to be a long column with the liquefied soil offering no support.

TESTS RESULTS AND ANALYSIS

Overall pile performance

The summary of the performance of the 9 piles in tests SB-02, SB-03 and SB-04 is shown in table 5. The test results of SB-05 are not included in the table, as the test was identical to SB-04 except that it did not have soil, and so the model piles act as cantilever struts. In the table, P_{cr} represents the elastic critical load of the pile treated as a column neglecting any support from the soil. It can be seen that in tests SB-02 and SB-04 all piles which should have failed did fail, whereas the piles in SB-03 should not have failed according to the buckling criterion, and did not fail. Pile failure in SB-02 cannot be positively attributed to the effects of axial load since lateral loads were also applied, whereas in test SB-04 the load was purely axial at failure. It can be concluded that tests SB-03 and SB-04 support the hypothesis of pile failure occurring for $P/P_{cr} \geq 1$. Figure 10 shows the slenderness ratio of the pile plotted against the mean axial stress. In the figure the yield stress line, Euler's elastic instability curve and Rankine's combined buckling curve are plotted. The graph has a close resemblance with the observed case histories of pile foundation performance during past earthquakes, as shown in figure 4.

Table 5: Performance of piles during the centrifuge tests

Test ID	Pile ID	Head mass kg	Max load P N	P/A MPa	L_{eff} (L_{eff}/r_{min})	P/ P_{cr}	Remarks
SB-02 Pile length = 160mm $r_{min}=3.1$ mm $A=9.7$ mm ²	1	1.96	768	79	$L_{eff}=355$ mm 114	0.97	Failed at 40-g during swing up
	2	1.56	642	65	$L_{eff}=350$ mm 113	1.01	Failed at 42-g during swing up
	3	1.26	617	63	$L_{eff}=345$ mm 111	0.97	Failed during earthquake
SB-03 Pile length = 180mm $r_{min}=3.1$ mm $A=11.2$ mm ²	4	0.60	294	26.3	$L_{eff}=372$ mm 120	0.5	Did not collapse
	5	0.45	220	19.7	$L_{eff}=370$ mm 119	0.35	Did not collapse
	6	0.23	113	10.1	$L_{eff}=370$ mm 119	0.22	Did not collapse
SB-04 Pile length = 180mm $r_{min}=3.1$ mm $A=11.2$ mm ²	7	1.25	610	54.5	$L_{eff}=420$ mm 135	1.04	Failed during earthquake
	8	1.78	872	78	$L_{eff}=445$ mm 144	1.48	Failed during earthquake
	9	4.68	2249	201	$L_{eff}=90$ mm 29	0.25	Did not collapse

Replication of mechanism

Figure 11 (a) shows the surface observation of the piles after test SB-02. It may be noted that the heads of the piles rotated. It is quite similar to visual observations of the piled building shown in figure 11 (b). The building is Kandla port tower in laterally spreading soil, which tilted by 15 degrees after the 2001 Bhuj earthquake (India). The pile that failed during the earthquake is shown in figure 11 (c) and the figure shows that the hinge formed at the top third of the pile. Figure 11 (d) shows the point of hinge formation in the failure of a three-storey R.C building revealed after excavation following the 1995 Kobe earthquake. There is a similarity between the locations of hinge formation in the centrifuge test and in the aftermath of real earthquakes. This demonstrates that the pile failure mechanisms observed in the field can be replicated using dynamic centrifuge modelling. It may be noted that the real piled buildings were in laterally spreading soil whereas the model piles in the experiments were in level ground. Thus the centrifuge tests point out that buckling can be a possible failure mechanism of piles in liquefiable soil sites.

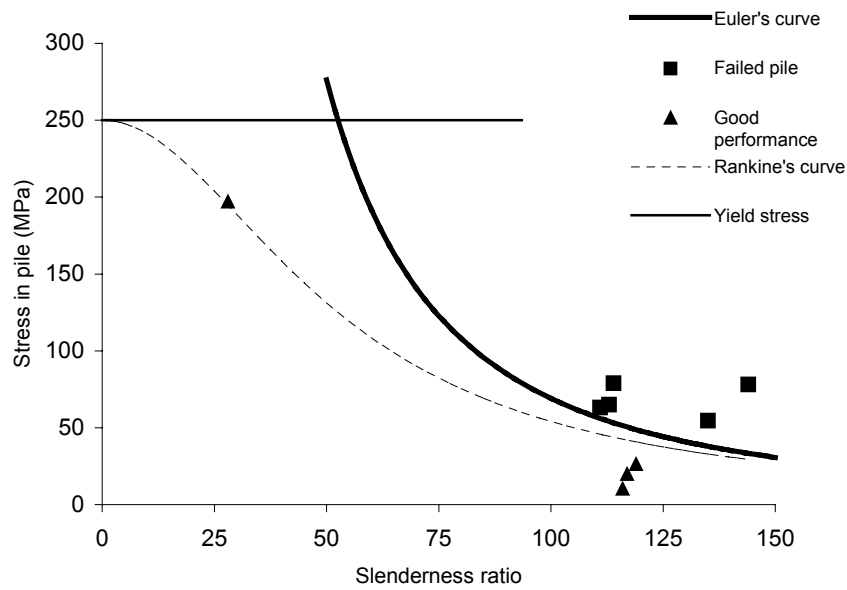


Figure 10: Performance of the piles in the tests SB-02, SB-03 and SB-04.

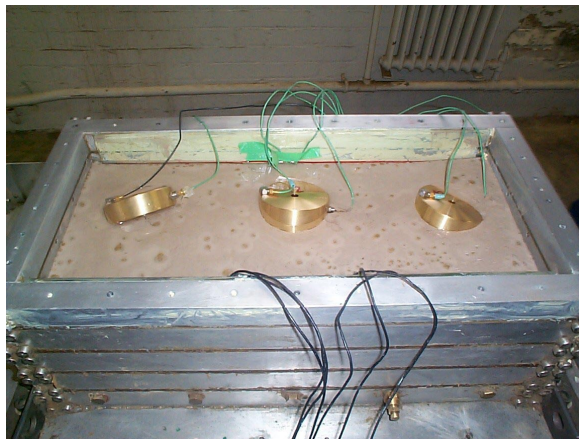


Figure 11 (a): Piles after the test in SB-02.



Figure 11 (b): Kandla tower after Bhuj earthquake, (Madabhushi et al 2001).



Figure 11 (c): Pile 3 after the earthquake.

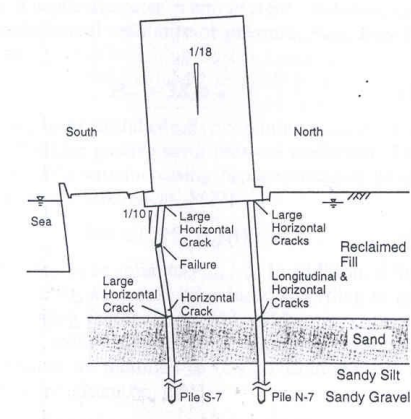


Figure 11 (d): Excavation of 3-storey R.C building (Tokimatsu et al, 1997).

Effect of axial load on pile foundation.

The present paper is intended to improve understanding of the effects of axial load on a pile during soil liquefaction and hence experiments SB-04 and SB-05 need to be discussed in more detail. It may be noted that no inertia force was acting on the pile head in the direction of buckling in tests SB-04 and SB-05 and hence the test results are the effects of axial load alone. Figure 12 (a) shows pile 7 partially revealed after the test during and figure 12 (b) shows the pile after excavation was complete. In test SB-05, an identical pile was tested in the absence of soil and figure 12 (c) shows that pile after the test. Similar forms of buckling are shown in figure 13 for pile 8, and thus we can conclude that this observation is repeatable.

In both tests, the piles buckled in the transverse direction, i.e. orthogonal to the direction of shaking. In test SB-04 the hinge formed about one third the way down the liquefiable soil whereas in test SB-05 the hinge formed at the bottom third of the pile in air.

Figure 14 shows the instrumentation layout with pore pressure transducer locations surrounding pile 8 and also in the free field. Figure 15 shows the free field traces of excess pore pressure. It may be noted that as the shaking starts the pore pressure rises in the soil starting from top and proceeding downwards. In every case, at a time of about 0.5 seconds in the history, or about 0.25 s after shaking started, the excess pore pressures δu in the free field reach a plateau. Figure 15 shows that in each case the plateau corresponds well with an estimate of the pre-existing effective vertical stress at the corresponding elevation, suggesting that σ'_v had fallen to zero. Between 0.5 s and 1.0 s in figure 15, the pile will have lost all lateral effective stress in a progressive fashion, top-down. When this advancing front reached a critical depth H_c given by equation 5, the pile would have become elastically unstable following equation 2.

$$H_c = \sqrt{\frac{\pi^2 EI}{4P}} \quad (5)$$

This instability will cause the pile to begin to move slowly sideways, pushing the soil. At the same time, the front of zero effective stress continues to advance swiftly downwards until the whole length of the pile is unsupported by the soil grains.

Resistance of liquefied soil

It is interesting to note the difference in mode shape of the piles in tests SB-04 in saturated sand and SB-05 in air. Figure 16 shows the mode shapes of the buckled pile in the two tests. Curvature being related to bending moment, the tests suggest that the lower part of the “liquefied” soil zone somehow offered resistance to the buckling pile and reduced bending moments in the lower two-thirds of its length. We might conclude that “liquefied” soil cannot prevent the initiation of buckling in an initially straight pile, but that some secondary support then becomes available.

Experimental work has been carried out by Takahashi et al (2002) to study the lateral resistance of piles in a liquefied soil. A pile was modelled as a buried cylinder that could be pushed laterally through “liquefied” soil. The displacement rate of the cylinder varied from 1mm/sec to 100mm/sec. The test results show that the initial resistance to movement is negligible at all rates of loading but that some lateral resistance was then mobilised after a certain amount of displacement. They further conclude that the higher the rate of loading the larger is the resistance. This supports the inference from the reduced curvature at depth in test SB-04 that “liquefied” soil can offer some shear resistance. Soil with $\sigma'_v = 0$ is often, and misleadingly, described as being in a state of “liquefaction”. As will shortly be demonstrated, the soil may have lost all its effective stress but has retained (or even increased) its original density. It is infinitely over-consolidated, denser than its critical density at its current effective stress level, highly dilatant, and can therefore regenerate considerable shear strength if it is subjected to ongoing undrained shear strains.

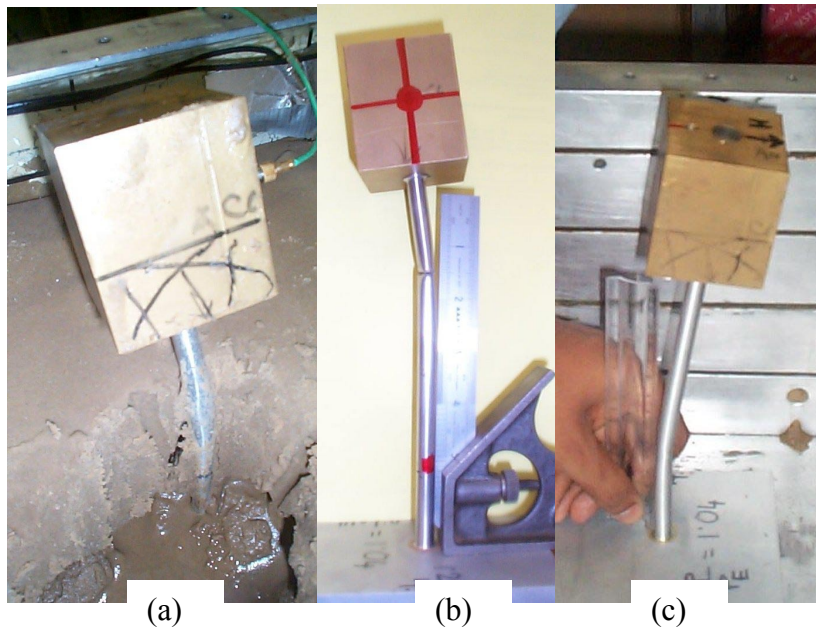
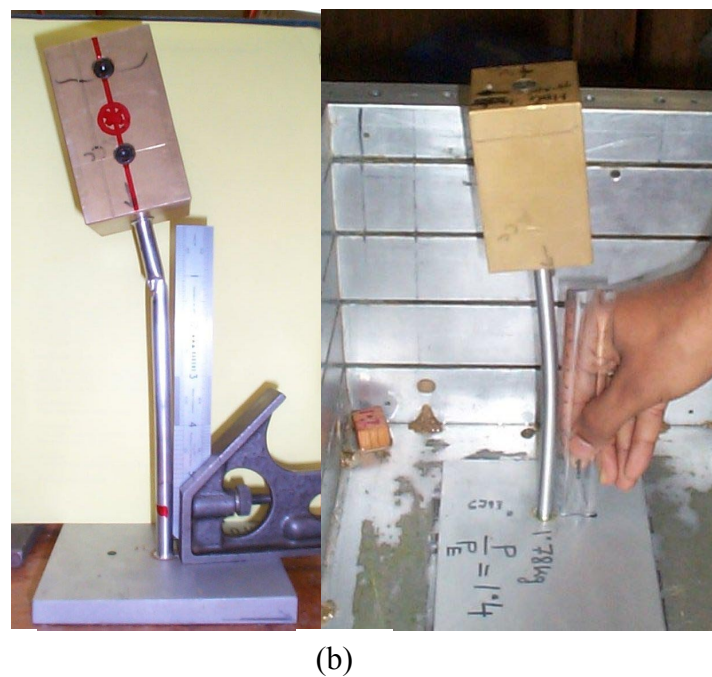


Figure12 (a): Mode of failure of pile 7 in test SB-04 during excavation.
Figure12 (b): Pile 7 after excavation.
Figure12 (c): Same pile in test SB-05.



Test 13 (a): Mode of failure of pile 8 in test SB-04.
Test 13 (b): Mode of failure of the same pile in test SB-05.

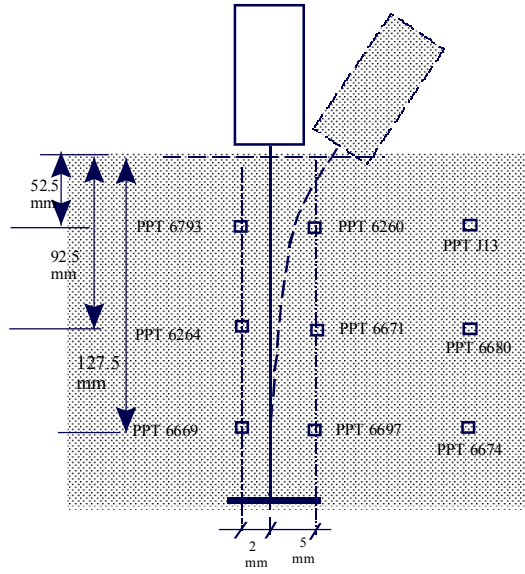


Figure 14: Instrumentation near the pile 8 in test SB-04.

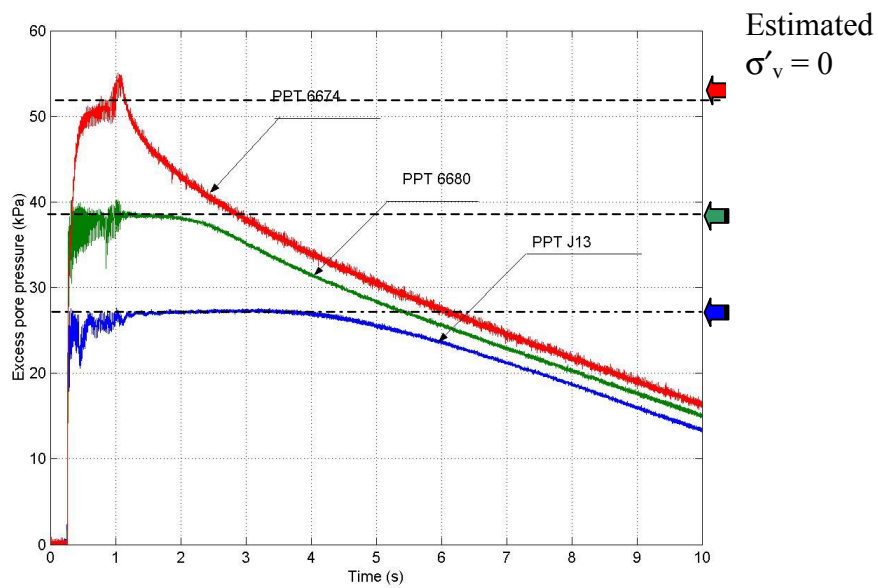


Figure 15: Plot of PPT data in far field of the pile.

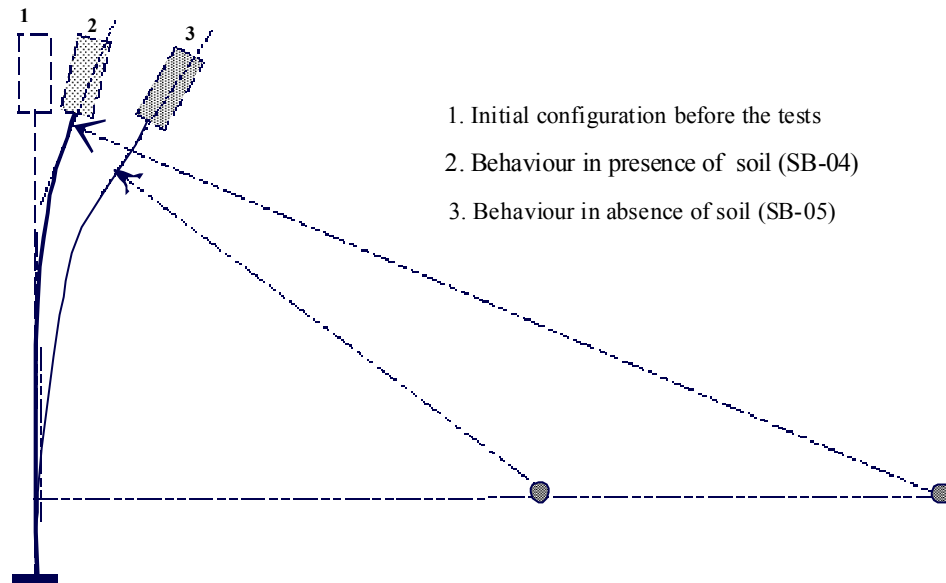


Figure 16: Comparison of the buckling mode shape of pile in tests SB-04 and SB-05.

It must be expected that the imposition of shear strains at low effective stresses in moderately dense soil will lead to an attempt to dilate, suppressed by the need for water to flow into the zone affected, which must then create a local reduction of pore fluid pressure. Figure 17, comparing the PPT traces at shallow depth in the near field of the pile (PPT 6260 in front of the pile, i.e. in the direction of eventual buckling; 6793 behind the pile) and the far field PPT J13, supports this hypothesis. At first, up to 0.4 s, the three PPTs record the same pressures rising to “liquefaction”. Then, until 1.0 s the PPT in front of the pile shows a circa 10 kPa reduction of pore pressure with additional sharper downward spikes at each earthquake cycle. The PPT behind the pile shows positive spikes which are at first out of phase with those in front and which then come in phase. The cyclic component of the PPT data behaviour is clearly related to the shaking, and therefore to motions orthogonal to the eventual direction of buckling. But the steady component of pore pressure reduction in front of the pile must be due to suppressed dilation as the pile begins to push the previously “liquefied” soil aside. Evidently the soil in that zone is liquefied no longer, but enjoys a vertical effective stress of between 10 and 20 kPa – enough for the pile to receive significant support – again, temporary.

By 1.0 s in the time record of figure 17, however, the pore pressure reduction in front of the pile has diminished, due to transient inflow presumably, to the point where the positive spikes take the pore pressure in front of the pile back up to the “liquefaction”

pressures of the far field. At that point the pile head load collapsed onto the surface of the saturated sand, when the pile plastically buckled. A tremendous *negative* spike of pore pressure is seen on PPT 6260 in front of the pile. By the time shaking ceases at 1.1 s this PPT is recording a steady 25 kPa pore pressure deficit compared with the “liquefied” far field, as the previously “liquefied” soil in the near field must now participate in the undrained bearing capacity of the load, acting as a rather tilted shallow foundation. Because it must carry load, and because it can generate as much effective stress as it needs to achieve that, its pore pressure drops correspondingly

Figure 18 shows that the ultimate displacement δ of the top of the pile, when normalised by the pile diameter D , gives a reference shear strain (Goh and O'Rourke, 1998; Takahashi et al, 2002) of $\delta/D = 200\%$. This magnitude of shear strain is quite sufficient for the achievement of a critical state in the shear zone. Since the far field remains “liquefied” beyond 3 s in the upper third of the soil layer, the “drained” critical state achieved in the upper third of the pile is one of zero effective stress and zero shear strength.

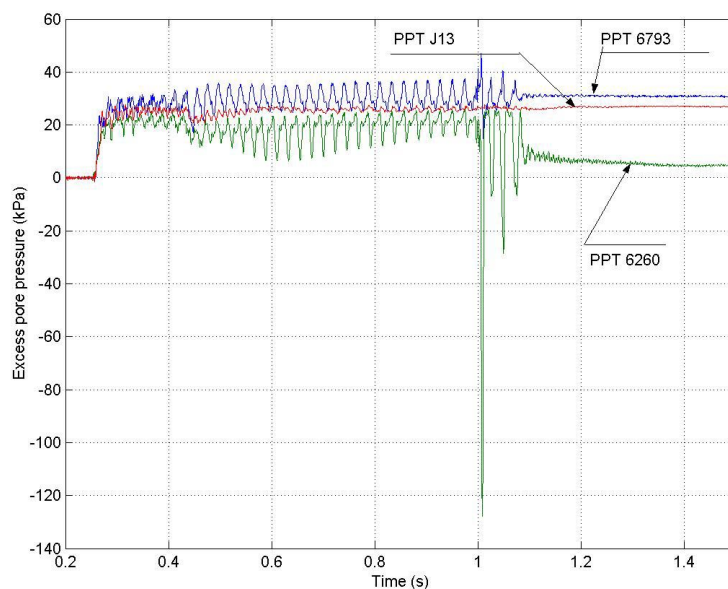


Figure 17: Near field and far field pore pressure measurements at 52.5mm depth.

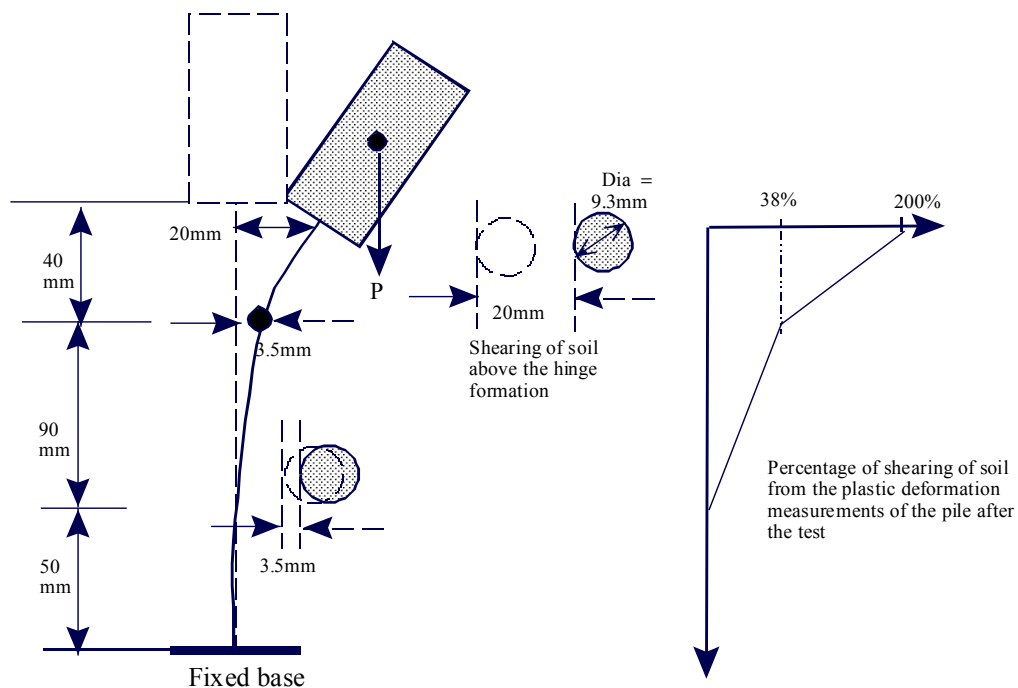


Figure 18: Plastic deformation measurements of pile 8 after test SB-04.

CONCLUSIONS

1. A similar failure mode as for full-scale piles observed after real earthquakes in liquefiable soil has been replicated with model piles in level ground in a centrifuge. Case histories and centrifuge test results match satisfactorily with a newly proposed theory of pile failure by buckling instability. The pile can buckle and push the soil; it is not necessary to invoke lateral spreading of the soil, which pushes the pile. This instability depends on the slenderness ratio (L_{eff}/r_{min}) of the pile exceeding a critical value in the liquefiable region. Once the surrounding soil has its effective stresses eliminated by an earthquake, a susceptible pile starts to buckle in the direction of least elastic stiffness. If the soil around the pile remains liquefied for long enough, the pile will suffer gross deformations and the superstructure will either tilt or deform.
2. Sufficient information has been obtained from centrifuge models to propose a hypothesis for pile-soil interaction during a buckling event. The buckling pile begins to shear the soil next to it, which will start to offer some temporary lateral resistance.

Even a loose-medium sand will have a rather large undrained shear strength. Such a sand could certainly apply the small restraint necessary to hold a buckling pile in quasi-static equilibrium. It achieves this by inducing a negative pore pressure increment in the shear zone relative to the “liquefied” far field. But the pore pressure difference creates a component of transient flow towards the pile. This flow feeds the dilation of the shearing soil, and reduces its strength as its density decreases. As the far field “liquefaction” pore pressures are reasserted, the lateral resistance of the soil reduces. It is the upper part of a liquefiable sand layer that remains longest in a state of “liquefaction” due to upward hydraulic gradients, and it is the upper part of the pile which displaces most, and which can fully soften the supporting soil adjacent to it. The buckling pile will suffer increasing loss of bending stiffness due to plastic yielding, so the restraint necessary to hold it in equilibrium will increase. The imbalance between reducing soil support, increasing bending moment created by lateral displacement of the pile cap, and deteriorating bending stiffness of the pile, inevitably leads to the formation of a relatively shallow plastic hinge or fracture, presaging dynamic collapse.

3. When saturated sand is shaken, its vertical effective stress can drop to zero as its pore pressure rises. This is sometimes spoken of as “liquefaction” and inverted commas have been used throughout the paper to indicate this sense of the word. But in both common speech, and in science, to liquefy means to transform to a liquid, and the defining characteristic of a liquid is that it does not offer any significant resistance to flow. In solid mechanics, flowing is shearing. So a liquefied soil would require no significant shear stress to produce large shear strains. The initial achievement of $\sigma'_v = 0$ in sand should therefore be spoken of as *suspension*, not liquefaction, since it is acknowledged that only super-loose sands (with an initial voids ratio exceeding e_{max} as conventionally determined) lose their undrained shear resistance completely.

4. Evidently, interlocking in a suspension of recently shaken sand grains with a relative density of 45% could provide enough shear resistance to prevent the development of the full-height buckle observed when a similar pile was tested in air. This resistance of a suspension to shearing has been shown to be due to suppressed dilation following interlocking. Pore pressures fall, and effective stresses rise, in

zones where the suspension is shearing. Correspondingly, this resistance is temporary as fluid drains into the shear zone from the suspension below. If the upward flow of water from below is maintained for long enough, the shearing suspension will dilate sufficiently for the grains to lose all their capacity to interlock. The fully sheared, fully dilated, fully softened, suspension will then have reached a critical state at zero effective stress and *high voids ratio*. It may then properly be described as liquefied. Liquefaction of sands therefore requires a source of water (from a suspension below the point of inspection), and a mechanism for mixing (i.e. shearing) excess water with the sand so as locally to exceed the critical voids ratio at zero effective stress, circa e_{max} .

5. After an earthquake, foundations on or in *suspended* sands will inevitably settle, together with the ground surface, as pore pressures dissipate but they should not suffer gross shear. If a zone of soil in contact with the foundation can *liquefy*, however, the foundation can cause unlimited soil shearing and the superstructure may collapse. Fear of soil liquefaction has been engrained in geotechnical engineers for two generations. A significant step forwards would be a moratorium on the use of “liquefaction” to describe any soil state than that of a heavy liquid.

ACKNOWLEDGMENTS

The authors are grateful to Mr Chris Collison and Mr John Chandler for technical support in doing the tests. Discussions with Mr Allan McRobie and support from Dr S.K.Haigh are gratefully acknowledged. The first author is thankful to Nehru Trust for Cambridge University and Cambridge Commonwealth Trust for financial help in doing the research.

NOTATION

L_{eff} : =Effective length of the pile in liquefiable region

r_{min} = minimum radius of gyration

I = Second moment area of the section

P_{cr} = Elastic critical load

A = Area of the section of the pile

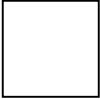
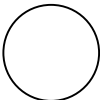
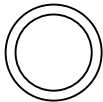
σ_f = Failure stress

σ_y = Yield stress

σ_{cr} = Elastic critical stress

L_{eff}/r_{min} = Slenderness ratio

APPENDIX-1

Pile section	I (second moment of area) and area of the section (A)	r_{min} (minimum radius of gyration)	Remarks
Square of sides a 	$I = \frac{a^4}{12}$ $A = a^2$	$r_{min} = \sqrt{\frac{I}{A}} = \frac{a}{\sqrt{12}}$	$r_{min} = 0.288 a$
Solid circular section (dia d) 	$I = \frac{\pi}{64} d^4$ $A = \frac{\pi}{4} d^2$	$r_{min} = \sqrt{\frac{I}{A}} = \frac{d}{4}$	$r_{min} = 0.25 d$
Tubular section Inside dia. (d_i) Outside dia. (d_o) 	$I = \frac{\pi}{64} (d_o^4 - d_i^4)$ $A = \frac{\pi}{4} (d_o^2 - d_i^2)$	$r_{min} = \sqrt{\frac{I}{A}} = \frac{\sqrt{d_o^2 + d_i^2}}{4}$	For practical purposes, $r_{min} = 0.35 d_o$ as $\frac{t}{d_o} \leq 0.01$ where, t=thickness

APPENDIX –2:

Failure of Showa bridge after 1964 Niigata earthquake:

Figure 19(a) and 19 (d) shows the failure of the 12 span 307m long Showa bridge. Figure 19(b) shows the post earthquake failure investigation and recovery of the damaged pile along with the soil investigation. The foundation consists of a row of piles connected laterally.

Design data of pile:

Length	25m
External diameter	609mm
Internal diameter	591mm
Material	Steel
E (Young's Modulus)	210GPa

Conventional pile capacity:

The pile capacity is estimated based on SPT values. Standard correlations have been used and the values are shown in figure 19 (c).

Shaft resistance

Layer 1 (outer)	565kN
Layer 2 (outer)	565kN

Base resistance

Plugged mechanism	2184kN
Unplugged mechanism	127kN

ULTIMATE PILE CAPACITY = 3314 kN

(Plugged mechanism)

ULTIMATE PILE CAPACITY = 2387 kN

(Unplugged mechanism)

ALLOWABLE LOAD IN PILE = 955 kN

(Using a factor of safety of 2.5)

Length in liquefiable zone = 10m

Structural properties of pile:

r_{min}	212mm
Moment of inertia (I)	$7.63 \times 10^8 \text{ mm}^4$
Effective length (L_{eff})	38m
Slenderness ratio	181

From the buckled shape (shown as original position in figure 19 (b)), it is clear that the pile had fixed-free boundary condition.

BUCKLING LOAD OF PILE = 1095kN

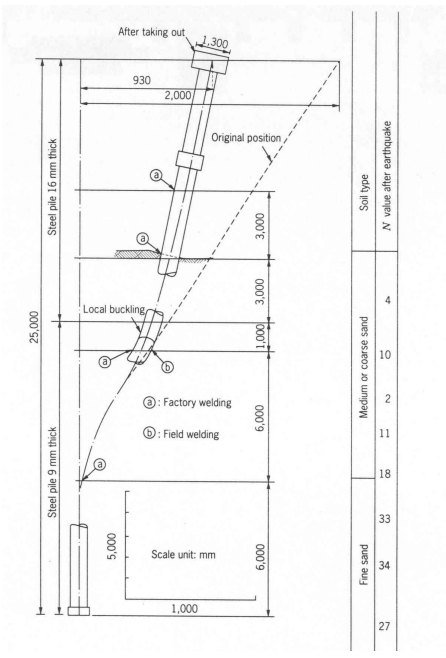


Figure 19(a): Collapse of Showa bridge, 1964 Niigata earthquake, Japan. Photo courtesy: NISEE website.

Figure 19 (b): Failed pile of Showa bridge showing the soil profile, Fukoka (1966).

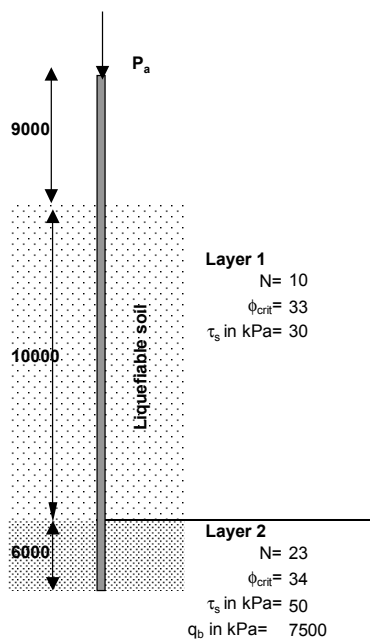


Figure 19(c): Design data to estimate the parameters in the analysis.

Figure 19 (d): Another view of the collapsed bridge. The figure shows the foundation system. Photo courtesy: EERC (University of California) website.

REFERENCES

1. Ayrton, W.E and Perry, J (1886). "On struts". *The Engineer*, **62**, pp 464.
2. Berrill, J.B., Christensen, S. A., Keenan, R. P., Okada, W. and Pettinga, J.R. (2001). Case Studies of Lateral Spreading Forces on a Piled Foundation. *Geotechnique* **51**, No. 6, pp 501-517.
3. Bond, A. J. (1989). Behaviour of displacement piles in over-consolidated clays. *PhD thesis*, Imperial College (UK).
4. B.S 8110: 1985, Structural Use of Concrete, *British Standard Institution*, London.
5. Fukoka, M (1966). Damage to Civil Engineering Structures, *Soils and Foundations*, Tokyo, Japan, Volume-6, No-2, March 1966, pp 45-52.
6. Goh, S and Rourke T.D (1999). Limit state model for soil-pile interaction during lateral spread. *Proc. 7th. U.S.-Japan Workshop on Earthquake Resistant Design of lifeline facilities and countermeasures against soil liquefaction. Seattle, WA.*
7. Hamada, M. (1992). Large ground deformations and their effects on lifelines: 1964 Niigata earthquake. *Case Studies of liquefaction and lifelines performance during past earthquake. Technical Report NCEER-92-0001, Volume-1, Japanese case studies, National Centre for Earthquake Engineering Research, Buffalo, NY.*
8. Hamada, M. (1992). Large ground deformations and their effects on lifelines: 1983 Nihonkai-Chubu earthquake. *Case Studies of liquefaction and lifelines performance during past earthquake. Technical Report NCEER-92-0001, Volume-1, Japanese case studies, National Centre for Earthquake Engineering Research, Buffalo, NY.*
9. Ishihara, K. (1997). Terzaghi oration: Geotechnical aspects of the 1995 Kobe earthquake. *Proceedings of ICSMFE, Hamburg*, pp 2047-2073.
10. JRA (1996). Japanese Road Association, *Specification for Highway Bridges, Part V, Seismic Design.*
11. Madabhushi, S.P.G., Schofield, A. N. and Lesley, S. (1998). A new Stored Angular Momentum based Earthquake Actuator. *Proceedings of Centrifuge '98 Tokyo*, 111-116.

12. Madabhushi, S.P.G., Patel, D. and Haigh, S.K. (2001). Draft version of “EEFIT report on observations of the 26th Jan 2001 Bhuj earthquake in India. *Institution of Structural Engineers, UK*.
13. Rankine, W.J.M (1866). Useful rules and tables. London.
14. Robertson, A (1925), “The strength of struts”, *ICE selected eng. Paper*, 28.
15. Soga, K. (1997). Chapter 8, “Geotechnical aspects of Kobe earthquake”, of *EEFIT report, Institution of Structural Engineers, UK*.
16. Schofield, A. N. (1981). Dynamic and Earthquake Geotechnical Centrifuge Modelling. *Proc. Int. Conf. Recent Advances in Geotechnical Earthquake Engineering and Soil Dynamics*, Vol. 3, 1081-1100.
17. Schofield, A. N. (1980). Cambridge Centrifuge operations. Twentieth Rankine Lecture. *Geotechnique*, London, England, Vol. **30**, 227-268.
18. Schofield, A. N. and Zeng, X (1992). Design and performance of an equivalent shear beam container for earthquake centrifuge modelling. *Technical report CUED/D-Soils/TR .275*.
19. Takahashi, A., Kuwano, Y., and Yano, A. (2002). Lateral resistance of buried cylinder in liquefied sand. *Proceedings of the International Conference on physical modelling in geotechnics, ICPMG-02, St. John's, Newfoundland, Canada*, 10-12th July.
20. Tan, F.S.C 1990). Centrifuge and Theoretical Modelling of Conical Footings on Sand. *PhD Thesis*, Cambridge University, U.K.
21. Tokimatsu K., Oh-oka Hiroshi, Satake, K., Shamoto Y. and Asaka Y. (1998). Effects of Lateral ground movements on failure patterns of piles in the 1995 Hyogoken-Nambu earthquake. *Proceedings of a speciality conference, Geotechnical Earthquake Engineering and Soil Dynamics III, ASCE Geotechnical Special publication No 75*, pp 1175-1186.
22. Tokimatsu K., Oh-oka Hiroshi, Satake, K., Shamoto Y. and Asaka Y. (1997). Failure and deformation modes of piles due to liquefaction-induced lateral spreading in the 1995 Hyogoken-Nambu earthquake”, *Journal Struct. Eng. AIJ (Japan)*, No-**495**, pp 95-100.
23. Tokimatsu K, Mizuno H. and Kakurai M. (1996). Building Damage associated with Geotechnical problems. Special issue of *Soils and Foundations*, Japanese Geotechnical Society, Jan 1996, pp 219-234.

24. Tomlinson, M.J (1977). *Pile Design and Construction Practice*, A viewpoint publication.